JCTC Journal of Chemical Theory and Computation

Article

Cite This: J. Chem. Theory Comput. 2019, 15, 3354−3361

pubs.acs.org/JCTC

Chasing the Full Free Energy Landscape of Neuroreceptor/Ligand Unbinding by Metadynamics Simulations

Riccardo Capelli,[*,†] Anna Bochicchio,[†,‡] GiovanniMaria Piccini,[¶,§] Rodrigo Casasnovas,[†,∥,#] Paolo Carloni,[*,†,○] and Michele Parrinello[¶,§,△]

[†]INM-9/IAS-5 Computational Biomedicine, Forschungszentrum Jülich, Wilhelm-Johnen-Straße, D-54245 Jülich, Germany

[¶]Department of Chemistry and Applied Biosciences, ETH Zürich, c/o USI Campus, Via Giuseppe Buffi 13, CH-6900 Lugano, Ticino, Switzerland

[§]Facoltà di Informatica, Istituto di Scienze Computazionali, Università della Svizzera italiana (USI), Via Giuseppe Buffi 13, CH-6900 Lugano, Ticino, Switzerland

[∥]JARA-HPC, Forschungszentrum Jülich, D-54245 Jülich, Germany

[○]Department of Physics, RWTH Aachen University, D-52078 Aachen, Germany

[△]Istituto Italiano di Tecnologia, Via Morego 30, I-16163 Genova, Italy

Supporting Information

ABSTRACT: Predicting the complete free energy landscape associated with protein−ligand unbinding may greatly help designing drugs with highly optimized pharmacokinetics. Here we investigate the unbinding of the iperoxo agonist to its target human neuroreceptor M_2, embedded in a neuronal membrane. By feeding out-of-equilibrium molecular simulations data in a classification analysis, we identify the few essential reaction coordinates of the process. The full landscape is then reconstructed using an exact enhanced sampling method, well-tempered metadynamics in its funnel variant. The calculations reproduce well the measured affinity, provide a rationale for mutagenesis data, and show that the ligand can escape via two different routes. The allosteric modulator LY2119620 turns out to hamper both escapes routes, thus slowing down the unbinding process, as experimentally observed. This computationally affordable protocol is totally general, and it can be easily applied to determine the full free energy landscape of membrane receptors/drug interactions.

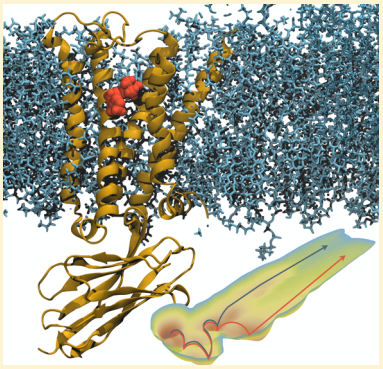

1. INTRODUCTION

Brain diagnostics rely mostly on Positron Emission Tomography (PET) imaging, where small molecules targeting specific neuroreceptors carry a short-lived isotope.[1] In their decay process, the isotopes emit a positron whose distribution reveals the position and receptors' expression levels inside the brain. Neurological diseases (from Schizophrenia to Parkinson's, from autism to brain tumors[2,3]) can be then readily revealed from receptors' maps. A great number of agonists and antagonists that target neuroreceptors for PET, called "tracers", have been designed,[4] yet little is known about their complex binding/unbinding processes. A detailed knowledge of these is of great importance, because it allows for designing ligands with a more predictable and safer behavior, modulating the affinity and reducing their residence time.[5]

In this work, we investigate *in silico* the molecular recognition process of a widely used tracer, iperoxo (Figure 1), inside the human muscarinic acetylcholine receptor M_2, a highly valuable target for neuroimaging. The M_2 receptor is a member of the G-protein coupled receptors (GPCRs) superfamily.[6] It regulates a large number of different functions in the human body, from modulation of cognition in the brain to motor processes.[7] It is also involved in neurological and neurodegenerative diseases like schizophrenia and Parkinson's.[8,9]

The description of such complex processes can be tackled on the computer by enhanced sampling techniques based on molecular dynamics simulations.[10] One of the most used methods is well-tempered metadynamics,[11,12] where the conformational space of a system can be studied enhancing the fluctuations along some set of relevant functions of the coordinates (called collective variables, CVs), depositing a bias that is dependent on the history of the system. This bias forces the system to explore new states, and, after reaching convergence, it is possible to recover the free energy surface projected along the chosen CVs. This was previously employed to unveil a variety of ligand binding/unbinding processes,[13,14] moving the problem to a clever identification of a suitable set of collective variables. Efficient metadynamics calculations of binding free energy differences in GPCRs, including M_2, was recently addressed using a single CV.[15] However, keeping pharmacological applications in mind, it is highly desirable to use a more general approach in which a larger number of CVs

Received: February 5, 2019
Published: March 26, 2019

Downloaded via UNIV DE LES ILLES BALEARS on May 25, 2020 at 15:33:38 (UTC).
See https://pubs.acs.org/sharingguidelines for options on how to legitimately share published articles.

© 2019 American Chemical Society

DOI: 10.1021/acs.jctc.9b00118
J. Chem. Theory Comput. 2019, 15, 3354−3361

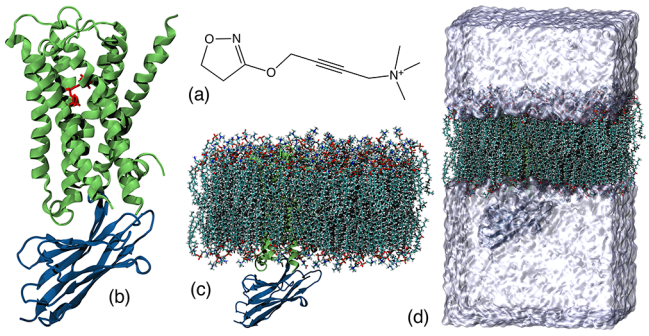

Figure 1. Human M_2 receptor in complex with its agonist iperoxo. (a) The ligand (4-(4,5-dihydro-1,2-oxazol-3-yloxy)but-2-ynyl-trimethylazanium) in 2D representation. (b) M_2 receptor (green) and its bound ligand, along with the Nb_{39} nanobody (blue). (c) Neuronal membrane with the receptor embedded in it. (d) The simulated system (~150,000 atoms) formed by ligand, receptor, membrane, water, and ions (the latter represented with a transparent surface for the sake of clarity).

is employed. In this way, the chemical aspects of binding/unbinding transitions and the intermediate state can be better described.[16]

Here, we present a new scheme that leads to a dramatic decrease in the CPU time needed to reach convergence, allowing the use of more than one CV. There is a practical limit in the number of CVs that can be implemented in metadynamics, because the convergence times scales exponentially with the number of the CVs. Considering this point, the number of CVs that is advisable to employ is usually no more than 3, which implies the need of wise dimensionality reduction methods. The problem of dimensionality reduction in complex phase-space transitions has recently seen an increasing number of approaches based on linear statistical projection of data,[17,18] as well as methods that involve machine learning/artificial intelligence approaches.[19] For computer-aided ligand design, the first kind of approach appears to be more useful: in a linear combination of different observables, the magnitude of the weights represents a straightforward estimation of the relative importance of the single components. In the case of more complex (i.e., nonlinear) combinations of those observables, recognizing the important ones can be a nontrivial (or even impossible) problem.

Here we propose to use such an approach based on a set of local descriptors, like distances and dihedral angles. These are determined by exploring putative unbinding pathways and candidate intermediate states using the so-called Ratchet&Pawl MD (rMD) simulations.[20,21] These are similar in spirit to steered MD simulations.[22] Analyzing those states, we were able to extract a set of 23 atom pair distances that describe ligand/receptor nonbonded interactions. The latter were projected in 3 CVs that separate well the intermediate states of the process by means of a recently developed data classification method, called Multi Class Harmonic Linear Discriminant Analysis (MC-HLDA).[17,18] This technique highlights the importance of every pair for the landscape description, keeping the physical meaning of the low-dimensional projection evident. Finally, using chemical intuition, we further reduced the number of CVs to 2, dramatically decreasing the converge time.

We use here the funnel variant of a well-tempered metadynamics method.[23] This allows for computation of accurate binding free energies at a lower computational cost. The calculations, based on the ligand/protein complex X-ray structure,[24] provide us with the full free energy landscape as a function of the two CVs. The resulting binding free energy (-13.6 ± 0.5 kcal/mol) agrees with that measured in saturation binding assays (-13.7 kcal/mol),[24] with a convergence time comparable to using a traditional approach with only one CV. Most importantly, our calculations allow for a highly precise description of the ligand binding events. In particular, we were able to confirm the ligand unbinding pathway emerged from rMD analysis and previous metadynamics simulations as a function of one CV[15] and to find a second pathway that involves the rearrangement of the extracellular loop 2 (ECL2, Figure 3).

The study of these pathways provides a rationale for previously reported mutagenesis data[25] and an atomic level explanation of the different kinetics of the tracer in the presence of an additional allosteric ligand, which enhances tracer's affinity for the receptor.[26] Hence, our method emerges as a powerful tool for accurate investigations of molecular recognition events of drug binding to human membrane receptors in laboratory realizable conditions.

2. RESULTS

Here we describe rMD and metadynamics simulations based on the equilibrated structure of the iperoxo/M_2 complex in a neuronal membrane mimic environment (see the SI). Here, M_2 is bound to a G-protein mimic nanobody. This allows the receptor to keep the active state conformation.[24]

Candidate Ligand Pathway and Intermediate States. Multiple rMD simulations may help identify intermediate states that the ligand finds on its way to unbinding at a moderate computational cost: we simulated 10 different unbinding events (stopping after the ligand is fully solvated) for a total of ~50 ns worth of simulation. The "ratcheting coordinate" gives a rough estimation of the progress of the unbinding event. Here, such a coordinate is the projection along the direction normal to the membrane of the distance between the center of mass of the ligand and the binding pocket.

By clustering the rMD trajectories, 7 major clusters were identified: the bound state, corresponding to the ligand's pose in the X-ray structure complex,[24] along with 6 different intermediates. We tested the stability of those states by performing MD simulations that were 50 ns long for every intermediate. Within this time scale only two states (**A** and **C**, Figure 2) remained stable. The others evolved toward directly into state **A** or **C** or passing through transient state **B** (Figure 2), which was visited several times in different simulations.

The picture emerging from this set of rMD simulations is that the overall process can be described by a rigid rotation of the ligand trimethylammonium group pivoting around D103. Starting from the crystallographic bound state (red in Figure 2), the ligand breaks its nonbonded interactions with hydrophobic residues $Q240^{(\text{side chain})}$, $F195^{(\text{backbone})}$, and $V111^{(\text{side chain})}$ while rotating around the axis formed by the alkyne bond (see Figure 2). The ligand ring simultaneously forms new H-bonds with $Y104^{(\text{side chain})}$, $S107^{(\text{side chain})}$, and $Y239^{(\text{side chain})}$ (state **A**, dark orange in Figure 2). At this point, the ligand further rotates along the salt bridge (Figure 2), finding a transient state (state **B**, light orange in Figure 2). Here, the ring interacts with $Y239^{(\text{side chain})}$ and $Y262^{(\text{side chain})}$. Next, the ligand reaches the last intermediate state (**C**, yellow in Figure 3). After, it breaks its nonbonded interactions with Y104 while maintaining the H-bonds with $Y239^{(\text{side chain})}$. The

DOI: 10.1021/acs.jctc.9b00118
J. Chem. Theory Comput. 2019, 15, 3354−3361

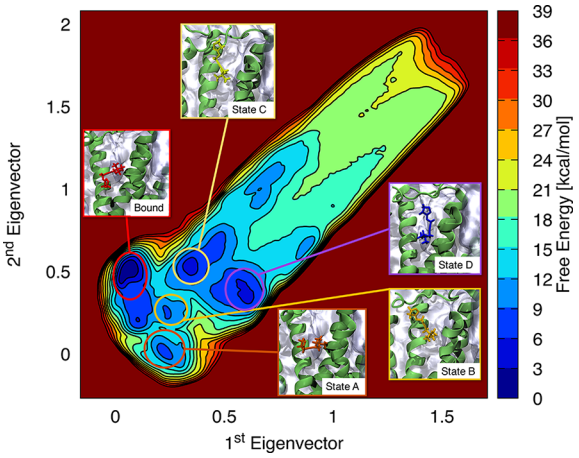

Figure 2. Free energy landscape of ligand unbinding. Free energy surface in function of the first 2 HLDA eigenvectors. The conformations of every free energy minimum of the ligand in the binding pocket are highlighted on the free energy surface.

ligand is now partially solvent exposed, forming H-bonds with ∼5 water molecules. Finally, it completely unbinds, and it becomes fully solvated. It assumes a conformation which is normal with respect to the membrane. Water molecules could freely go back and forth from the extracellular side to the binding site during the unbinding events. Along with the lipids, they do not play a particular role during the process. The same observations hold in all simulations performed here.

The simulations allowed the identification of 23 local descriptors able to identify all the different intermediate and transient states (see Table S1). These where chosen here as distances between atom pairs involved in the observed nonbonded interaction (i.e., hydrogen bonds and salt bridges) conserved for more than 20% of the simulation time in each state.

In conclusion, the simulations show a rigid rotation of the ligand with the pivot given by the salt bridges between the ligand trimethylammonium group and D103. Consistently, the salt bridge is maintained in all four states, representing the pivot of the unbinding transition.

CVs Identification. We aim at finding optimal collective variables starting from the 23 descriptors identified as essential transition parameters during the unbiased MD runs described above. To reduce the dimensionality of our descriptors, we exploited HLDA (details in Methods and the SI). HLDA allows packing into low dimensional yet efficient CV large sets of state descriptors that capture the essential dynamics of the process. The only information required by the algorithm is simple statistical quantities, namely means and multivariate variances, collected during unbiased runs in the reference states.

In other words, we estimate the average and the fluctuations of all the local descriptors (i.e., by computing them in an equilibrium MD simulation) in all the states of interest and manipulate them in order to obtain a lower dimensional projection of the conformational space that can be used in our enhanced sampling techniques (details in Methods and the SI). The main advantage of HLDA with respect to other similar dimensionality reduction techniques is the fact that HLDA exploits the information about the fluctuations of the descriptors in the free energy basins (see the SI), highlighting the relative importance of every component in the linear combination that constitutes our final CVs. For instance, other techniques like PCA,[27] PLS-DA,[28] and LDA[29] rescale the data by their standard deviation to ensure the similarity of the distributions, losing part of the information.

In the construction of the HLDA we consider four states, the stable bound state, **A**, and **C**. We added state **B** because, although it is not stable, it appeared to be an important transit step in the evolution of the unbinding process. Being such that the state was relatively short-lived if compared to states **A** and **C**, it was not possible to simulate it in an equilibrium MD run for enough time. This happens because, during the unbiased MD runs, the ligand jumps to both states **A** and **C**. Therefore, the fluctuation matrix for this state was constructed by combining information coming from all the simulations that explored this state, while for the other 3 states the standard procedure was used (see Methods). According to HLDA, out of these states 3 optimal CVs were constructed. In order to speed up convergence, we neglected the CV with the lowest associated eigenvalue since in our rMD dynamics a strong correlation between the trajectory projection on the lowest and the second highest eigenvalues was seen (see Figure S2).

Metadynamics Simulation. With this choice of CVs, we performed a metadynamics simulation with 8 different walkers. After 1 μs of simulation we have seen a large number of binding/unbinding events in all the walkers, and we reached convergence (see Figures S3 and S4). Our metadynamics run shows that all of the rMD intermediate states are relative free energy minima and that the bound state is the absolute minimum (Figure 2). However, another intermediate state (**D** in Figure 2) emerges from our calculated free energy landscape. The ligand here forms H-bonds with $Y266^{(\text{side chain})}$ and $Y104^{(\text{side chain})}$, as emerging from a 50 ns-long MD simulation performed on **D**: we have an H-bond with $Y266^{(\text{side chain})}$ and $Y104^{(\text{side chain})}$. In addition, ECL2 (Figure 3) changes its conformation with respect to the bound state: It rotates having as pivot W162 and N183. During this rearrangement, the $W90^{(\text{backbone})}$-$T229^{(\text{backbone})}$ and $N246^{(\text{side chain})}$-$Y177^{(\text{side chain})}$ H-bonds are disrupted, and the $T262^{(\text{side chain})}$-$C176^{(\text{backbone})}$, $W258^{(\text{backbone})}$-$E175^{(\text{side chain})}$, and $D173^{(\text{side chain})}$-$Y83^{(\text{side chain})}$ are formed (Instead, in both states a salt bridge between R189 and D97 and a hydrogen bond $T247^{(\text{side chain})}$-$F191^{(\text{backbone})}$ are maintained.). The rearrangement of the extracellular loop forces the ligand to continue the rotation described above having D103 as a pivot to find a way to reach the solvated state.

The presence of intermediate state **D** leads us to suggest the existence of two different pathways from the bound to the solvated state (Figure 3). The first is that identified by rMD (see Section above). In the second one, as we have just seen, the rearrangement of the extracellular loop forces the ligand to perform a further rotation before reaching the solvent (state **D**).

As a last point, we computed the free energy difference between the bound state of our system and the free ligand in the solvent. The free energy difference between the unbound and the bound states obtained was $\Delta G = -13.6 \pm 0.5$ kcal/mol, in a good agreement with the experimental value of $\Delta G = -13.7$ kcal/mol.[24]

3. DISCUSSION

We have presented a protocol to study thermodynamics and the intermediate states progression of protein−ligand unbinding processes. As an example, we have focused on a clinically

DOI: 10.1021/acs.jctc.9b00118
J. Chem. Theory Comput. 2019, 15, 3354−3361

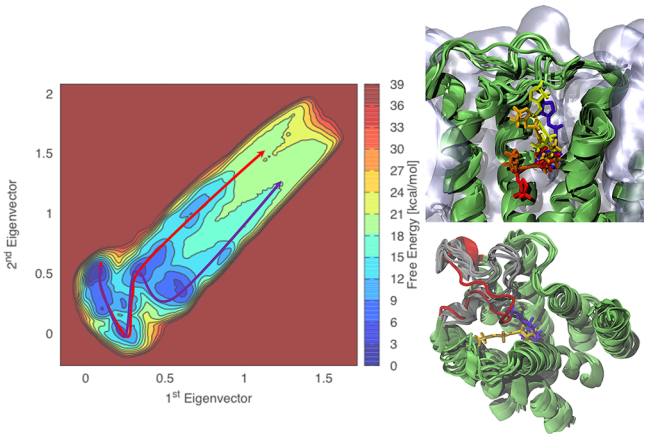

Figure 3. Two pathways of unbinding. Left: schematic representation of the unbinding pathways for iperoxo in the M2 receptor on its free energy surface (left panel). The first unbinding pathway (red arrow) is the one predicted by exploratory rMD simulations. The second unbinding pathway (violet arrow) is the one found after the rearrangement of the extracellular loop during metadynamics simulations. Top right: Bound (red), states **A** (dark orange), **B** (light orange), **C** (yellow), and **D** (violet) for iperoxo (licorice representation) inside the M_2 receptor (cartoon representation). Water and ions have been removed for the sake of clarity. Bottom right: cartoon representation of the M_2 receptor with the ligand iperoxo in states **C** and **D**. In gray, the position of the ECL2 in the bound state and states **A**, **B**, and **C**. The position of the loop when the system is in state **D** is in red. This change in the receptor conformation forces the ligand to rotate from state **C** (yellow) to state **D** (violet) to reach the solvent.

approved tracer binding to a neuroreceptor for PET applications. This is iperoxo in the M_2 receptor, for which experimental structural information is available.[24]

To describe the full free energy landscape associated with the process, we have adopted here a two-step strategy. First, we integrated data from an out-of-equilibrium technique (rMD) with a modified data classification analysis method (HLDA) to capture the relevant chemical features of the process. Then, with a well-defined and reliable equilibrium method (Funnel Metadynamics) we investigated the thermodynamics of our protein−ligand (un)binding process. The calculations show that the bound state is the pose in the X-ray structure[24] and allow identifying the intermediate (**A**, **C**, **D**) and transient (**B**) states (Figure 2).

We calculated relevant observables that can be compared with experimental data,[24] obtaining a good agreement ($\Delta G_{sim} = -13.6 \pm 0.5$ kcal/mol vs $\Delta G_{exp} = -13.7$ kcal/mol). A similar value of ΔG was obtained with a single CV.[15] However, here we have a much more detailed description and deeper insight of the behavior of the ligand. In particular, Y104 reveals itself as a key residue for the ligand binding process by forming important stabilizing interactions in the intermediates states **A** and **B**. In addition, D103 plays a fundamental role for the conformational changes of iperoxo in the entire unbinding process and in the bound state. Indeed, D103 is the pivot for the rotation of iperoxo (Figures 3 and S7). These results provide a rationale for binding selectivity experiments, which shows that both groups are key residues for agonists binding.[25] Most importantly, the reconstruction of the full energy landscape points to two different escape pathways for this ligand (Figure 3). The first was identified by rMD simulations and previous computational works.[15] It does not involve significant changes in the structure of the receptor. In contrast, the second pathway, not emerging from the other simulations, does involve a complex rearrangement of the ECL2 loop (Figure 3), which leads in turn to intramolecular H-bonds breakages.

The presence of allosteric ligands−used to enhanced the ligand's affinity[26]−is expected to affect both escape routes. Indeed, visual inspection of the X-ray structure of the receptor in the presence not only of the iperoxo tracer but also of one allosteric ligand, called LY2119620 (the only experimental structure available with both the ligands),[24] shows that (i) the first pathway is directly blocked by the allosteric modulator itself (see Figure S6) and (ii) the conformational rearrangement of the extracellular loop needed to open the second pathway is hindered (see Figure S6). So, directly or indirectly the allosteric modulator hampers the ligand's unbinding from the receptor. This provides a rationale for the large decrease (more than 1 order of magnitude) in k_{off} upon addition of the allosteric ligand.[30] We plan to apply this technique also to the full system (receptor+orthosteric ligand+allosteric ligand), to study also quantitatively the allosteric effect on the ligand binding.

Next, we stress the efficiency of our computational protocol: we reached convergence on 2 different CVs with a computational effort comparable to the one needed to converge on the same system on a single CV.[15] This is particularly important in large systems (Figure 1) like GPCRs, which constitute a target for more than 30% of FDA drugs.[31] This protocol can be straightforwardly applied to similar pharmacologically relevant biomolecules, including other transmembrane proteins. Indeed, one can expect that the number of intermediate states in an unbinding transition should be similar to the one found for this system. One can then foresee the possibility of applying the dimensionality reduction given by HLDA to properly describe unbinding events. Keeping pharmacological applications in mind, another important point is the usage of a more realistic neuronal membrane model. The membrane composition was shown to change structure, dynamics, and thermodynamics of GPCRs in a significant way.[32,33]

Keeping future ligand design applications in mind, our calculations allow also for the identification of important chemical groups for the binding and unbinding processes. First, a charged group, like trimethylammonium, should be present to interact with D103. Indeed, other agonists such as acetylcholine and Oxotremorine M[34,35] contain such a group. Furthermore, the atom O2 in the ring (see Figure S9) is involved in structural determinants (the distances d_1, d_3, d_8, and d_{19}), which contribute significantly to our CVs. Similarly, the distances involving N2 (d_2, d_5, d_9, d_{17}, and d_{18}) are important for our CVs. Those functional groups emerge as important also experimentally in the work of Schrage et al.,[34] where a comparison of different possible decorations is shown, and the common point of all those 3 decorations is the charged part and the presence of the oxygen and nitrogen atoms. In another work,[35] the authors start from a functionalized benzene scaffold and a quaternary ammonium salt (to form a salt bridge with D103) with different carbon chains spacers. From all the candidates shown, only those containing an oxygen atom at the same distance of the one present in the iperoxo showed good docking scores in the active state, confirming the hints given by HLDA analysis.

One of the future planned applications of this technique consists of including explicitly full free energy landscape

DOI: 10.1021/acs.jctc.9b00118
J. Chem. Theory Comput. 2019, 15, 3354−3361

information as shown in Russo et al.[36] for protein/ligand binding, including structures from the transition state to lower the free energy barriers. Another possible extension is to use free energy landscape information combined with the optimization of the ligand conformation itself employing metadynamics.[37,38]

In conclusion, we have shown the possibility to integrate new statistically accurate information toward a more precise drug design. All the nonbonded interaction data obtained by enhanced sampling can give a large number of constraints in current drug design techniques, possibly raising the success rate in designing a new molecule that can bind the system studied. In the future, we plan to extend our approach to the calculation of kinetic constants of ligand binding/unbinding, where metadynamics[39] and other techniques like variationally enhanced sampling[40] may be exploited.

4. MATERIALS AND METHODS

System Preparation. The structure of the human M_2/iperoxo complex at 3.5 Å resolution (PDB access code 4MQS[24]) was obtained in the presence of a G-protein-mimic, the Nb_{39} nanobody. The latter stabilizes the receptor in its active conformation.[24] We kept the G-protein-mimic in our simulations to avoid that the active state collapses to the inactive one, as observed in the recent MD and accelerated MD simulations.[41] The crystallographic structure contains some missing loops in the intracellular region that we choose not to reconstruct for the lack of a suitable template (>20% sequence identity) among other neuroreceptors. In particular, residue C457 is missing; this cysteine is conserved among a huge number of GPCR and is involved in palmitoylation, which can affect a huge number of functions of neuroreceptors.[42] In the M_2 receptor, the effect of palmitoylation was experimentally studied, showing that nonpalmitoylated cysteine does not show a different affinity for G-protein.[43] More importantly for our study, it was also shown that the absence of this cysteine does not affect the ligand binding process in the M_2 muscarinic receptor.[44]

The receptor was inserted into membrane bilayers following the orientation of the OPM database.[45] The lipids composition was chosen to represent that of a model neuronal membrane[46] (i.e., 48% cholesterol, 16% phosphatidylcholine (DPPC and POPC), 16% phosphatidylethanolamine (DOPE), 14% sphyngomielin (SM 18:0), 4% phosphatidylserine (DOPS), and 2% phosphatidylinositol (SOPC)). This may be important for the overall fold of the protein and ligand poses.[32] The system was solvated with explicit water molecules, and the appropriate number of sodium and chloride ions was added to neutralize the total charge and reproduce a physiological salt concentration of 150 mM, similar to the one used in affinity experiments.[24] The final systems contained ∼150.000 atoms, and the dimensions of the resulting simulation box were 112 × 113 × 149 $Å^3$. The dimension along the Z axis was chosen such that complete solvation can be achieved when the ligand dissociates from the M_2 receptor. The simulations were performed using GROMACS 2016.4.[47] The protein, membrane, counterions, and water were described by the AMBER ff14SB force field,[48] the CHARMM-GUI[49] and Slipids,[50−53] Joung and Cheatham force fields,[54] and TIP3P,[55] respectively. The force field of the ligand was the generalized AMBER force field (GAFF).[56] The atomic charges, after a geometry optimization on the Cartesian coordinates (to avoid the lack of the dihedral definition in the atoms involved in the triple covalent bond), were obtained by the restrained electric potential fitting method (RESP)[57] with molecular electric potentials obtained in the HF/6-31G* level of theory. Quantum chemical calculations were performed with Gaussian 09.[58] A cutoff distance of 12 Å was used for the van der Waals and short-range electrostatic interactions, and the long-range electrostatic interactions were computed with the particle-mesh Ewald summation method[59] using a grid point spacing of 1 Å. Long-range dispersion corrections to the pressure and potential energy were considered.[60]

MD Simulations. We first equilibrated the lipid tails. With all other atoms fixed, the lipid tails were energy minimized for 1000 steps using the steepest descent algorithm and melted with an NVT run for 0.5 ns at 310 K (37 °C). In a constant pressure run, we equilibrated the system to a stable volume, fixing only the positions of the protein and the ligand. During this part of the run, that lasted a total of 10 ns, we observed that after 5 ns the volume of the box was fluctuating around its equilibrium value without any canonical drift. We then released the protein restraints for a further 0.5 ns keeping the pressure of 1 bar and physiological temperature (i.e., 310 K). After these minimization and equilibration procedures, the production MD simulations were performed on the systems for 0.7 μs. The temperature was kept constant using velocity rescaling thermostat[61] with solvent, solute, and membrane coupled to separate heat baths with coupling constants of 0.5 ps. The pressure was maintained constant with a semi-isotropic scheme, so that the pressure in the membrane plane was controlled separately from the pressure in the membrane normal direction, and the Parrinello−Rahman barostat[62,63] was applied with a reference pressure of 1 bar, a coupling constant of 2 ps, and a compressibility of 4.5×10^{-5} bar^{-1}.

rMD Simulations. To study the unbinding path of our ligand we exploited Ratchet&Pawl MD[20,21] (details in the SI). Saleh et al.[15] used the projection along the direction normal to the membrane of the distance between a conserved tryptophan and the ligand center of mass as CV in their metadynamics simulation. Inspired by this, we defined as our ratcheting coordinate the projection along the direction normal to the membrane of the distance between the center of mass of the heavy atoms of iperoxo ligand and the center of mass of the binding pocket (residues TYR104, SER107, VAL111, PHE195, TYR239). We fixed the bias factor to k = 500 kJ/mol/nm and the final ratchet coordinate to r_{final} = 3 nm. The rMD term was implemented via the PLUMED 2.3 plugin.[64]

HLDA Dimensionality Reduction. We made use of the HLDA technique to reduce the number of collective variables from 23 (the number of our local descriptors) to 3 (the number of the bound, intermediate, and transient states minus one). We analyzed the unbiased MD simulation started from all the rMD identified states obtaining the time series of the local descriptors. We then computed averages and standard deviations of the local descriptors in all the states, and then we applied the HLDA protocol (details in the SI). This dimensionality reduction approach has been used first by Fisher[29] and adapted to chemical physics problems.[17,18]

Metadynamics Simulations. Here we use a variant of well-tempered metadynamics,[11,12] called Funnel Metadynamics.[23] In this variant, the ligand is free to explore its conformational space inside the binding pocket, but in the proximity of the interface between the solvent and the receptor, a funnel-shaped potential is present. The potential confines the ligand in a small region of space outside the

DOI: 10.1021/acs.jctc.9b00118
J. Chem. Theory Comput. 2019, 15, 3354−3361

receptor. The loss of degrees of freedom given by the funnel potential can be corrected analytically[23,65] (details in the SI). We started the conic region of the funnel potential 13 Å above the crystallographic position of the ligand, reaching the cylindrical part with a radius of 1 Å to 22 Å above the binding pocket. The cylindrical part of the funnel is 18 Å long to ensure the absence of residual electrostatic interaction of the ligand with the membrane or the receptor at its end (see Figure S5). We performed a Multiple-Walkers[66] Well-Tempered Metadynamics, implementing 8 different walkers, each one depositing a Gaussian of height 1.2 kJ/mol every ps with a bias factor of $\gamma = 24$ for a total simulation time of 1 μs (125 ns per replica). Metadynamics was implemented via the PLUMED 2.3 plugin.[64] All the obtained free energy surfaces were reweighted a posteriori using the algorithm presented by Tiwary and Parrinello.[67]

■ ASSOCIATED CONTENT

Supporting Information

The Supporting Information is available free of charge on the ACS Publications website at DOI: 10.1021/acs.jctc.9b00118.

Details on HLDA, RatchetMD, and additional data (PDF)

■ AUTHOR INFORMATION

Corresponding Authors

*E-mail: r.capelli@fz-juelich.de.
*E-mail: p.carloni@fz-juelich.de.

ORCID

Riccardo Capelli: 0000-0001-9522-3132
GiovanniMaria Piccini: 0000-0002-3511-4281
Paolo Carloni: 0000-0002-9010-0149

Present Addresses

‡Department of Biology, Friedrich-Alexander-Universität Erlangen-Nürnberg, Staudstraße 5, D-91058 Erlangen, Germany.
#Department of Chemistry, Universitat de les Illes Balears, Crta. de Valldemossa km 7.5, E-07122 Palma de Mallorca, Baleares, Spain.

Funding

The authors gratefully acknowledge the computing time granted through JARA-HPC on the supercomputer JURECA at Forschungszentrum Jülich (Project ID: jias58) and acknowledge the JSC for the computing time on the supercomputer JURECA Booster module. This project has received funding from the European Union's Horizon 2020 Research and Innovation Programme under Grant Agreement No. 785907 (HBP SGA2).

Notes

The authors declare no competing financial interest.

■ ACKNOWLEDGMENTS

The authors thank Emiliano Ippoliti, Luca Maggi, and Giulia Rossetti for useful discussions.

■ REFERENCES

(1) Phelps, M. E.; Mazziotta, J. C. Positron Emission Tomography: Human Brain Function and Biochemistry. *Science* **1985**, *228*, 799–809.
(2) Pasquini, J.; Ceravolo, R.; Qamhawi, Z.; Lee, J.-Y.; Deuschl, G.; Brooks, D. J.; Bonuccelli, U.; Pavese, N. Progression of tremor in early stages of Parkinson's disease: a clinical and neuroimaging study. *Brain* **2018**, *141*, 811–821.
(3) Gambhir, S. S. Molecular imaging of cancer with positron emission tomography. *Nat. Rev. Cancer* **2002**, *2*, 683–93.
(4) Honer, M.; Gobbi, L.; Martarello, L.; Comley, R. A. Radioligand development for molecular imaging of the central nervous system with positron emission tomography. *Drug Discovery Today* **2014**, *19*, 1936–1944.
(5) Copeland, R. A. The drug-target residence time model: A 10-year retrospective. *Nat. Rev. Drug Discovery* **2016**, *15*, 87–95.
(6) Caulfield, M. P.; Birdsall, N. J. M. International Union of Pharmacology. XVII. Classification of Muscarinic Acetylcholine Receptors. *Pharmacol. Rev.* **1998**, *50*, 279–290.
(7) Wess, J.; Eglen, R. M.; Gautam, D. Muscarinic acetylcholine receptors: Mutant mice provide new insights for drug development. *Nat. Rev. Drug Discovery* **2007**, *6*, 721–733.
(8) McOmish, C.; Pavey, G.; McLean, C.; Horne, M.; Dean, B.; Scarr, E. Muscarinic receptor binding changes in postmortem Parkinson's disease. *J. Neural Transm.* **2017**, *124*, 227–236.
(9) Scarr, E.; Dean, B. Muscarinic receptors: do they have a role in the pathology and treatment of schizophrenia? *J. Neurochem.* **2008**, *107*, 1188–95.
(10) Schneider, S.; Provasi, D.; Filizola, M. The Dynamic Process of Drug-GPCR Binding at Either Orthosteric or Allosteric Sites Evaluated by Metadynamics. *Methods Mol. Biol.* **2015**, *1335*, 277–94.
(11) Laio, A.; Parrinello, M. Escaping free-energy minima. *Proc. Natl. Acad. Sci. U. S. A.* **2002**, *99*, 12562–12566.
(12) Barducci, A.; Bussi, G.; Parrinello, M. Well-tempered metadynamics: A smoothly converging and tunable free-energy method. *Phys. Rev. Lett.* **2008**, *100*, 020603.
(13) Saleh, N.; Saladino, G.; Gervasio, F. L.; Haensele, E.; Banting, L.; Whitley, D. C.; Sopkova-de Oliveira Santos, J.; Bureau, R.; Clark, T. A Three-Site Mechanism for Agonist/Antagonist Selective Binding to Vasopressin Receptors. *Angew. Chem., Int. Ed.* **2016**, *55*, 8008–8012.
(14) Li, J.; Jonsson, A. L.; Beuming, T.; Shelley, J. C.; Voth, G. A. Ligand-Dependent Activation and Deactivation of the Human Adenosine A2A Receptor. *J. Am. Chem. Soc.* **2013**, *135*, 8749–8759.
(15) Saleh, N.; Ibrahim, P.; Saladino, G.; Gervasio, F. L.; Clark, T. An Efficient Metadynamics-Based Protocol to Model the Binding Affinity and the Transition State Ensemble of G-Protein-Coupled Receptor Ligands. *J. Chem. Inf. Model.* **2017**, *57*, 1210–1217.
(16) Schmidtke, P.; Javier Luque, F.; Murray, J. B.; Barril, X. Shielded hydrogen bonds as structural determinants of binding kinetics: Application in drug design. *J. Am. Chem. Soc.* **2011**, *133*, 18903–18910.
(17) Mendels, D.; Piccini, G.; Parrinello, M. Collective Variables from Local Fluctuations. *J. Phys. Chem. Lett.* **2018**, *9*, 2776–2781.
(18) Piccini, G.; Mendels, D.; Parrinello, M. Metadynamics with Discriminants: a Tool for Understanding Chemistry. *J. Chem. Theory Comput.* **2018**, *14*, 5040–5044.
(19) Schneider, E.; Dai, L.; Topper, R. Q.; Drechsel-Grau, C.; Tuckerman, M. E. Stochastic Neural Network Approach for Learning High-Dimensional Free Energy Surfaces. *Phys. Rev. Lett.* **2017**, *119*, 150601.
(20) Marchi, M.; Ballone, P. Adiabatic bias molecular dynamics: A method to navigate the conformational space of complex molecular systems. *J. Chem. Phys.* **1999**, *110*, 3697–3702.
(21) Tiana, G.; Camilloni, C. Ratcheted molecular-dynamics simulations identify efficiently the transition state of protein folding. *J. Chem. Phys.* **2012**, *137*, 235101–235101.
(22) Izrailev, S.; Stepaniants, S.; Isralewitz, B.; Kosztin, D.; Lu, H.; Molnar, F.; Wriggers, W.; Schulten, K. *Computational molecular dynamics: challenges, methods, ideas*; Springer: 1998; pp 39–65, DOI: 10.1007/978-3-642-58360-5_2.
(23) Limongelli, V.; Bonomi, M.; Parrinello, M. Funnel metadynamics as accurate binding free-energy method. *Proc. Natl. Acad. Sci. U. S. A.* **2013**, *110*, 6358–6363.

(24) Kruse, A. C.; Ring, A. M.; Manglik, A.; Hu, J.; Hu, K.; Eitel, K.; Hbner, H.; Pardon, E.; Valant, C.; Sexton, P. M.; Christopoulos, A.; Felder, C. C.; Gmeiner, P.; Steyaert, J.; Weis, W. I.; Garcia, K. C.; Wess, J.; Kobilka, B. K. Activation and allosteric modulation of a muscarinic acetylcholine receptor. *Nature* **2013**, *504*, 101−106.
(25) Gregory, K. J.; Hall, N. E.; Tobin, A. B.; Sexton, P. M.; Christopoulos, A. Identification of orthosteric and allosteric site mutations in M 2 muscarinic acetylcholine receptors that contribute to ligand-selective signaling bias. *J. Biol. Chem.* **2010**, *285*, 7459−7474.
(26) Tränkle, C.; Weyand, O.; Schröter, A.; Mohr, K. Using a Radioalloster to Test Predictions of the Cooperativity Model for Gallamine Binding to the Allosteric Site of Muscarinic Acetylcholine M2 Receptors. *Mol. Pharmacol.* **1999**, *56*, 962−965.
(27) Pearson, K., LIII LIII. On lines and planes of closest fit to systems of points in space. *Philos. Mag. (1798−1977)* **1901**, *2*, 559−572.
(28) Barker, M.; Rayens, W. Partial least squares for discrimination. *J. Chemom.* **2003**, *17*, 166−173.
(29) Fisher, R. A. The use of multiple measurements in taxonomic problems. *Annals of Eugenics* **1936**, *7*, 179−188.
(30) Croy, C. H.; Schober, D. A.; Xiao, H.; Quets, A.; Christopoulos, A.; Felder, C. C. Characterization of the Novel Positive Allosteric Modulator, LY2119620, at the Muscarinic M2 and M4 Receptors. *Mol. Pharmacol.* **2014**, *86*, 106−115.
(31) Hopkins, A. L.; Groom, C. R. The druggable genome. *Nat. Rev. Drug Discovery* **2002**, *1*, 727−730.
(32) Cao, R.; Rossetti, G.; Bauer, A.; Carloni, P. Binding of the antagonist caffeine to the human adenosine receptor hA2AR in nearly physiological conditions. *PLoS One* **2015**, *10*, e0126833.
(33) Lyman, E.; Higgs, C.; Kim, B.; Lupyan, D.; Shelley, J. C.; Farid, R.; Voth, G. A. A role for a specific cholesterol interaction in stabilizing the Apo configuration of the human A(2A) adenosine receptor. *Structure* **2009**, *17*, 1660−1668.
(34) Schrage, R.; Seemann, W.; Klöckner, J.; Dallanoce, C.; Racké, K.; Kostenis, E.; De Amici, M.; Holzgrabe, U.; Mohr, K. Agonists with supraphysiological efficacy at the muscarinic M2 ACh receptor. *Br. J. Pharmacol.* **2013**, *169*, 357−370.
(35) Fish, I.; Stößel, A.; Eitel, K.; Valant, C.; Albold, S.; Huebner, H.; Möller, D.; Clark, M. J.; Sunahara, R. K.; Christopoulos, A.; Shoichet, B. K.; Gmeiner, P. Structure-Based Design and Discovery of New M2 Receptor Agonists. *J. Med. Chem.* **2017**, *60*, 9239−9250.
(36) Russo, S.; Callegari, D.; Incerti, M.; Pala, D.; Giorgio, C.; Brunetti, J.; Bracci, L.; Vicini, P.; Barocelli, E.; Capoferri, L.; Rivara, S.; Tognolini, M.; Mor, M.; Lodola, A. Exploiting Free-Energy Minima to Design Novel EphA2 Protein-Protein Antagonists: From Simulation to Experiment and Return. *Chem. - Eur. J.* **2016**, *22*, 8048−8052.
(37) Spitaleri, A.; Ghitti, M.; Mari, S.; Alberici, L.; Traversari, C.; Rizzardi, G.-P.; Musco, G. Use of Metadynamics in the Design of isoDGR-Based $\alpha v\beta 3$ Antagonists To Fine-Tune the Conformational Ensemble. *Angew. Chem.* **2011**, *123*, 1872−1876.
(38) Di Leva, F. S.; Tomassi, S.; Di Maro, S.; Reichart, F.; Notni, J.; Dangi, A.; Marelli, U. K.; Brancaccio, D.; Merlino, F.; Wester, H.-J.; Novellino, E.; Kessler, H.; Marinelli, L. From a Helix to a Small Cycle: Metadynamics-Inspired $\alpha v\beta 6$ Integrin Selective Ligands. *Angew. Chem., Int. Ed.* **2018**, *57*, 14645−14649.
(39) Casasnovas, R.; Limongelli, V.; Tiwary, P.; Carloni, P.; Parrinello, M. Unbinding Kinetics of a p38 MAP Kinase Type II Inhibitor from Metadynamics Simulations. *J. Am. Chem. Soc.* **2017**, *139*, 4780−4788.
(40) McCarty, J.; Valsson, O.; Tiwary, P.; Parrinello, M. Variationally Optimized Free-Energy Flooding for Rate Calculation. *Phys. Rev. Lett.* **2015**, *115*, 070601.
(41) Miao, Y.; Nichols, S. E.; Gasper, P. M.; Metzger, V. T.; McCammon, J. A. Activation and dynamic network of the M2 muscarinic receptor. *Proc. Natl. Acad. Sci. U. S. A.* **2013**, *110*, 10982−7.
(42) Naumenko, V. S.; Ponimaskin, E. Palmitoylation as a Functional Regulator of Neurotransmitter Receptors. *Neural Plast.* **2018**, *2018*, 5701348.
(43) Hayashi, M. K.; Haga, T. Palmitoylation of muscarinic acetylcholine receptor m2 subtypes: reduction in their ability to activate G proteins by mutation of a putative palmitoylation site, cysteine 457, in the carboxyl-terminal tail. *Arch. Biochem. Biophys.* **1997**, *340*, 376−382.
(44) Van Koppen, C. J.; Nathanson, N. M. The Cysteine Residue in the Carboxyl-Terminal Domain of the m2Muscarinic Acetylcholine Receptor Is Not Required for Receptor-Mediated Inhibition of Adenylate Cyclase. *J. Neurochem.* **1991**, *57*, 1873−1877.
(45) Lomize, M. A.; Pogozheva, I. D.; Joo, H.; Mosberg, H. I.; Lomize, A. L. OPM database and PPM web server: Resources for positioning of proteins in membranes. *Nucleic Acids Res.* **2012**, *40*, D370−D376.
(46) Chan, R. B.; Oliveira, T. G.; Cortes, E. P.; Honig, L. S.; Duff, K. E.; Small, S. A.; Wenk, M. R.; Shui, G.; Di Paolo, G. Comparative lipidomic analysis of mouse and human brain with Alzheimer disease. *J. Biol. Chem.* **2012**, *287*, 2678−2688.
(47) Abraham, M. J.; Murtola, T.; Schulz, R.; Páll, S.; Smith, J. C.; Hess, B.; Lindahl, E. GROMACS: High performance molecular simulations through multi-level parallelism from laptops to supercomputers. *SoftwareX* **2015**, *1−2*, 19−25.
(48) Maier, J. A.; Martinez, C.; Kasavajhala, K.; Wickstrom, L.; Hauser, K. E.; Simmerling, C. ff14SB: Improving the Accuracy of Protein Side Chain and Backbone Parameters from ff99SB. *J. Chem. Theory Comput.* **2015**, *11*, 3696−3713.
(49) Jo, S.; Kim, T.; Vidyashankara, I. G.; Wonpil, I. CHARMM-GUI: A Web-Based Graphical User Interface for CHARMM. *J. Comput. Chem.* **2008**, *29*, 1859−1865.
(50) Ermilova, I.; Lyubartsev, A. P. Extension of the slipids force field to polyunsaturated lipids. *J. Phys. Chem. B* **2016**, *120*, 12826−12842.
(51) Jämbeck, J. P. M.; Lyubartsev, A. P. Derivation and systematic validation of a refined all-atom force field for phosphatidylcholine lipids. *J. Phys. Chem. B* **2012**, *116*, 3164−3179.
(52) Jämbeck, J. P. M.; Lyubartsev, A. P. An extension and further validation of an all-atomistic force field for biological membranes. *J. Chem. Theory Comput.* **2012**, *8*, 2938−2948.
(53) Jämbeck, J. P. M.; Lyubartsev, A. P. Another piece of the membrane puzzle: Extending slipids further. *J. Chem. Theory Comput.* **2013**, *9*, 774−784.
(54) Joung, I. S.; Cheatham, T. E. Determination of Alkali and Halide Monovalent Ion Parameters for Use in Explicitly Solvated Biomolecular Simulations. *J. Phys. Chem. B* **2008**, *112*, 9020−9041.
(55) Jorgensen, W. L.; Chandrasekhar, J.; Madura, J. D.; Impey, R. W.; Klein, M. L. Comparison of simple potential functions for simulating liquid water. *J. Chem. Phys.* **1983**, *79*, 926−935.
(56) Wang, J.; Wolf, R. M.; Caldwell, J. W.; Kollman, P. A.; Case, D. A. Development and Testing of a General Amber Force Field. *J. Comput. Chem.* **2004**, *25*, 1157−1174.
(57) Bayly, C. I.; Cieplak, P.; Cornell, W. D.; Kollman, P. A. A well-behaved electrostatic potential based method using charge restraints for deriving atomic charges: The RESP model. *J. Phys. Chem.* **1993**, *97*, 10269−10280.
(58) Frisch, M. J.; Trucks, G. W.; Schlegel, H. B.; Scuseria, G. E.; Robb, M. A.; Cheeseman, J. R.; Scalmani, G.; Barone, V.; Petersson, G. A.; Nakatsuji, H.; Li, X.; Caricato, M.; Marenich, A. V.; Bloino, J.; Janesko, B. G.; Gomperts, R.; Mennucci, B.; Hratchian, H. P.; Ortiz, J. V.; Izmaylov, A. F.; Sonnenberg, J. L.; Williams-Young, D.; Ding, F.; Lipparini, F.; Egidi, F.; Goings, J.; Peng, B.; Petrone, A.; Henderson, T.; Ranasinghe, D.; Zakrzewski, V. G.; Gao, J.; Rega, N.; Zheng, G.; Liang, W.; Hada, M.; Ehara, M.; Toyota, K.; Fukuda, R.; Hasegawa, J.; Ishida, M.; Nakajima, T.; Honda, Y.; Kitao, O.; Nakai, H.; Vreven, T.; Throssell, K.; Montgomery, J. A., Jr; Peralta, J. E.; Ogliaro, F.; Bearpark, M. J.; Heyd, J. J.; Brothers, E. N.; Kudin, K. N.; Staroverov, V. N.; Keith, T. A.; Kobayashi, R.; Normand, J.; Raghavachari, K.; Rendell, A. P.; Burant, J. C.; Iyengar, S. S.; Tomasi, J.; Cossi, M.;

DOI: 10.1021/acs.jctc.9b00118
J. Chem. Theory Comput. 2019, 15, 3354−3361

Millam, J. M.; Klene, M.; Adamo, C.; Cammi, R.; Ochterski, J. W.; Martin, R. L.; Morokuma, K.; Farkas, O.; Foresman, J. B.; Fox, D. J. *Gaussian09*; 2009.
(59) Essmann, U.; Perera, L.; Berkowitz, M. L.; Darden, T.; Lee, H.; Pedersen, L. G. A smooth particle mesh Ewald method. *J. Chem. Phys.* **1995**, *103*, 8577−8593.
(60) Shirts, M. R.; Mobley, D. L.; Chodera, J. D.; Pande, V. S. Accurate and Efficient Corrections for Missing Dispersion Interactions in Molecular Simulations. *J. Phys. Chem. B* **2007**, *111*, 13052−13063.
(61) Bussi, G.; Donadio, D.; Parrinello, M. Canonical sampling through velocity rescaling. *J. Chem. Phys.* **2007**, *126*, 014101.
(62) Parrinello, M.; Rahman, A. Crystal Structure and Pair Potentials: A Molecular-Dynamics Study. *Phys. Rev. Lett.* **1980**, *45*, 1196−1199.
(63) Parrinello, M.; Rahman, A. Polymorphic transitions in single crystals: A new molecular dynamics method. *J. Appl. Phys.* **1981**, *52*, 7182−7190.
(64) Tribello, G. A.; Bonomi, M.; Branduardi, D.; Camilloni, C.; Bussi, G. PLUMED 2: New feathers for an old bird. *Comput. Phys. Commun.* **2014**, *185*, 604−613.
(65) Allen, T. W.; Andersen, O. S.; Roux, B. Energetics of ion conduction through the gramicidin channel. *Proc. Natl. Acad. Sci. U. S. A.* **2004**, *101*, 117−122.
(66) Raiteri, P.; Laio, A.; Gervasio, F. L.; Micheletti, C.; Parrinello, M. Efficient Reconstruction of Complex Free Energy Landscapes by Multiple Walkers Metadynamics. *J. Phys. Chem. B* **2006**, *110*, 3533−3539.
(67) Tiwary, P.; Parrinello, M. A Time-Independent Free Energy Estimator for Metadynamics. *J. Phys. Chem. B* **2015**, *119*, 736−742.

DOI: 10.1021/acs.jctc.9b00118
J. Chem. Theory Comput. 2019, 15, 3354−3361